Indian J. Applied & Pure Bio. Vol. 39(1), 307-323 (2024). **ISSN: 0970-2091**
A Web of Science Journal

Potential of Biologically synthesized Zinc oxide Nanoparticles in controlling Fruit rot on Chilli

Amitha Ganapathy B, Nandish G, Sowmya H V and Thippeswamy Basaiah

Department of P.G. Studies and Research in Microbiology, Bioscience Complex, Kuvempu University, Jnanasahyadri, Shankaraghatta-577 451 (India)

Abstract

Chilli fruit rot disease is a major problem in vegetable-growing areas worldwide. Chemical fungicides are commonly used to control fungal diseases, but there is growing interest in using biologically synthesized Zinc Oxide nanoparticles (ZnO NPs) due to their unique properties. In this study, ZnO NPs were synthesized using *Aspergillus niger*-Sg9 and *Fusarium oxysporum*-Db4 fungi and evaluated against chilli fruit rot caused by *Colletotrichum fructicola (C. fructicola)*. The NPs were characterized using various techniques, and their efficacy was tested under in vitro, in vivo, and field conditions. Results showed that Sg9 and Db4 ZnO NPs at a concentration of 1000 ppm inhibited the growth of *Colletotrichum fructicola* by 89.61% and 85.71%, respectively, outperforming the standard control fungicide Propiconazole (73.16%). Sg9 ZnO NPs also demonstrated 98.46% growth suppression when applied before pathogen inoculation. The findings of the study indicated that biologically synthesized ZnO NPs offer a promising alternative for controlling chilli fruit rot disease.

Key words : Biosynthesized, ZnO nanoparticles (ZnO NPs), Fruit Rot, *Colletotrichum fructicola*.

Recent developments in science and technology have led to research scientists' attempts to produce nanoparticles with a size of less than 100 nm due to their numerous advantages in various field[20,33]. Nanoparticles can be created by chemical, physical and biological, processes. Out of these, the biological technique appears to be the most efficient and environmentally benign because the other two methods' usage is restricted by the presence of harmful substances. Additionally, scientists frequently use biological techniques to create high-yielding, inexpensive, and nontoxic nanoparticles[24,30]. The biological approach was used with the aid of physiologically active products produced by Fungi, Bacteria, Yeasts and plant that are ideal sources for the creation of nanoparticles[9,16]. Because of their nature of tolerance, superior metal bioaccumulation capability, and high binding capacity, the fungi were typically chosen over bacteria. Fungi have several uses because they generate large amounts of enzymes, easily scale up processes, are economically viable, and are simple to handle biomass[13].

Zinc (Zn), which is the sole metal

included in the six types of enzymes such as lyases, oxidoreductases, transferases, hydrolases, isoesterases, and ligases. It is often the second most prevalent metal after iron[13]. Research studies on the synthesis, characteristics, and characterization of ZnO NPs have drawn a lot of interest recently because of their potential uses[13,30]. Particularly, the synthesis of ZnO NPs has attracted considerable interest because of their broad antibacterial action, eco-friendliness, and simplicity. This nanoparticle has been used in a variety of industries, including the rubber, pharmaceutical, textile, biosensor, and cosmetics industries[1,26] Additionally, this technique for making nanoparticles is more beneficial since it makes nanoparticles at low pH, pressure, and temperature[2].

[1] According to several studies *Aspergillus niger* is an opportunistic, pervasive fungus that is a mycotoxigenic food and feed contaminant, notably of several vegetables, fruits, nuts, legumes, and grains[7]. In addition, the fungus causes invasive aspergillosis in immuno-compromised individuals and greatly raises morbidity and death rates in newborns[7]. Whereas the soil-borne plant pathogen *Fusarium oxysporum* causes vascular wilts in a variety of ornamentals, crops, and woodlands. *Aspergillus niger* -affected crop areas commonly employ the fungicides Thiram, Zineb, Captan, Benomyl, and Thiabendazole[1,7]. Similar antifungal drugs against *F. oxysporum* include carbendazim, thinovit, thiophanate-methyl, and benomyl[7]. The effective control of these fungi remains unsatisfactory despite the administration of these site-specific antifungal medicines. Synthetic pesticides are poisonous and cause toxicity in crop fields when used repeatedly. ZnO NPs are one such potential eco-safe antifungal agent that urgently warrants development. The current study examined the synthesis, and characterisation of ZnO NPs using the *Aspergillus niger* and *Fusarium oxysporum* and also the application of ZnO NPs on plant pathogens.

Molecular characterization of fungi isolated from soil sample :

Fungal culture was isolated and were characterized molecularly using 18s rRNA sequencing. The CTAB technique was applied to extract fungal DNA, and the quality and quantity of DNA was evaluated using 0.8% agarose gel electrophoresis and UV spectro-photometer. PCR was performed on the isolated DNA using ITS primers (ITS-1 and ITS-4). The sequences acquired from PCR samples were processed using BioEdit and processed with Blast. Further the sequence was eventually submitted to Gen Bank at the National Centre for Biotechnology Information.

Biosynthesis and purification of zinc oxide nanoparticles (ZnO NPs) :

Following the method of Raliya and Tarafdar 2014[25], metal tolerant fungi were cultivated in a flask with 1000 mL of customized Malt Extract Glucose Yeast Extract Peptone (MGYP) medium. The flasks were incubated in a rotating shaker at 30 °C at 150 rpm for 72 h. The culture filtrate was supplemented with 1 mM zinc nitrate, and it was shaken at 150 rpm for 48 h at 28°C. The mixture turned into opaque white precipitate which indicated that ZnO NPs were generated. The same mixture was centrifuged at 18,000 rpm for 5 min[12]. The precipitates were washed with alcohol followed by three times with distilled water and then dried for 4 h at 70°C. The ZnO NPs

were then crushed to powder and calcined for 1 hour at 500 °C [14]. The obtained fine powder was collected and stored at room temperature in an airtight glass vial for further studies.

Characterization of Biosynthesized ZnO NPs :

A) *UV-Visible Spectrophotometer (Uv-Vis) and UV-Visible Diffuse Reflectance Spectra (DRS) Analysis:* The optical properties of ZnO NPs were characterized by UV-Vis Spectroscopy (Systronics) and band gap energy spectra by UV-Vis diffuse reflectance spectra (UV-Vis DRS, Shimadzu 2450) in the wavelength range of 200 to 900 nm by using the reference material barium sulphate ($BaSO_4$), at 100 nm/min of a scanning speed.

B) *FTIR:* An FT-IR (IRTracer 100 AH, Shimadzu, Japan) spectroscope was used to examine the functional group in the synthesized ZnO NPs. The sample was made by combining ZnONPs coupled with potassium bromide (KBr) in a hydraulic press, followed by drying to eliminate the moisture content. The instrumentation was set built using Lab Solution software (Version 100) and infrared spectra was recorded at a resolution of 4 cm^{-1} in the range 350-7800 cm^{-1}.

C) *X-Ray Diffractometer (XRD):* XRD (M/s. Rigaku, Ultima 4, Tokyo, Japan) was used to determine the phase of synthesized and standard ZnO NPs. The data was compared to identify standard data from the Joint Committee on Powder Diffraction Standards (JCPDS Card No. 36-1451). Using Debye-Scherrer's formula (equation 1), the XRD pattern of ZnO NPs was employed to estimate the average particle size[31].

$$D = \frac{k\lambda}{\beta cos\theta} \quad (1)$$

Where 'D' is the ZnO NPs crystallite size, 'k' is the shape factor (0.9), is the wavelength of X-ray (1.54) Cu K radiation, is the Bragg angle form 2 value of intensity peak from XRD pattern, and is the full width half maximum of the diffraction from XRD pattern of ZnO NPs.

D) *Scanning electron microscope (SEM) - element detection sensor (EDS):* Using SEM (Carl Zeiss, EVO 10, Germany) and an EDS (Oxford Instruments, X-MaxN 80, United Kingdom), the surface morphology and elemental detection of synthesized ZnO NPs were addressed.

E) *Dynamic Laser Scattering and Zeta Potential:* To assess the size and surface charge of the nanoparticles, zeta potential and dynamic light scattering were evaluated using a particle size analyzer (Zetasizer) (Malvern, nano 383, England). The cuvette containing the nanoparticle solution was filled to the top third of its volume before being set within the zeta sizer's dynamic light scattering chamber. The experiment was performed with a scattering angle of 90° and a temperature of 25 °C. Dispersion and refra ctive index of ZnO NPs were tuned to 1.365 and 1.330, with a viscosity of 0.8872 Cp. Using Malvern software (Version 7.12), it was possible to determine the average particle diameter (nm) for all ZnO Nps from the intensity graph[12].

Evaluation of ZnO NPs on control of chilli fruit rot Disease :

Recently, ZnO NPs attracted plenty of attention due to their antibacterial and

antifungal potential. Regarding assessing the beneficial effects of ZnO NPs on the control of chilli fruit infections, multiple factors need to be investigated, including the specific diseases, mode of administration and nanoparticle concentration. Overall, ZnO NPs exhibited as a potential tool for disease control in chilli fruits, further research is needed to ensure their efficacy, safety, and sustainability in farming practices. Before presenting NPs for broad implementation in agriculture, it is necessary to perform field trials to evaluate the ecological effects of their use. In addition, it strongly encouraged local agricultural extension services or researchers in the area to obtain particular advice tailored to specific regions and the target diseases. Thus, the *in vitro* and *in vivo* screening of ZnO NPs was performed against *C. fructicola*.

A) *In vitro Screening of ZnO NPs against Colletotrichum fructicola:* *C. fructicola* were grown on PDA for 7 days at 25°C. The agar dilution method with minor changes was used for antifungal testing[21]. Sterilized PDA media with various concentrations of ZnO NPs and NP-free solution (25,50,100, 250, 500, 750,1000, and 2000 PPM) were loaded onto sterilized petri dishes (9 cm diameter). A plug of fungal mycelia (1 cm) was extracted from the edge of the 7-day-old plate and placed in the center of each petri dish, after which it was incubated at 25°C. At 15 days, the diameter of fungal growth was measured to determine the curative effects of ZnO NPs treatment. The sizes were measured in millimeters (mm) and each test was performed in triplicate. The growth inhibition rate was measured once mycelia in control plates grew to the edge of the petri dish. The following formula 2 was used to determine the inhibition rate where (h) is the diameter of the fungal mycelial growth on the plate treated with ZnO NPs and (H) is the diameter of the growth on the control plate.

$$\text{Inhibition rate (\%)} = (H\ h) / H\ 100 \qquad (2)$$

B) *In vivo Screening of ZnO NPs against Colletotrichum fructicola:* The three highest concentrations (500, 750, and 1000 PPM) of NP were determined using the poison food technique against *C. fructicola* on detached fruits. Following surface sterilization for 30 seconds in 0.1 percent $HgCl_2$ healthy fruits from susceptible chillies were completely rinsed in sterilized distilled water. On sterile tissue paper, the fruits which were already surface sterilized were then air dried. The test fruits were separated into two groups for NP application pre and post 48 h of spore inoculation. The test fruits were punctured at 2-3 specific spots and immersed in different quantities of ZnO NPs. The fungicides served as a standard check, while sterilized distilled water served as a control. After 30 min, the dipped fruit was air dried on sterile paper tissue and 6 µL of conidial suspension (1×10^{-6} spores/ml) was dabbed onto the wound. The pathogen spore suspensions were created by harvesting spores from a 7 day old fungal culture cultivated on PDA in 5-10 mL of sterilized distilled water. The treated fruits were incubated at 25°C in moist chambers maintained under plastic tray containers with wet blotting papers. After 8 days of inoculation, the disease progression was assessed by measuring the length of the hampered portion's lesion[21]. Ten fruits per replication were kept for each treatment, and the experiment was carried out in triplicates using a Completely Randomised Design (CRD). The

spore suspension was made by scraping the fungal growth from the PDA pure culture plate with a sterilized scalpel and distilled water. The spore suspension was filtered using three layers of sterilized cheese cloth. The spores were counted with a hemacytometer and the concentration was adjusted to 2.5×10^6 spores/ml by diluting it with water. There were two different experiment sets. Different ZnO NPs concentrations (500 ppm, 750 ppm, and 1000 ppm) were sprayed 7 days prior to spore inoculation in the first group and 7 days thereafter in the second set. Two sprays were administered at 15-day intervals. The fungicide acted as standard check, while sterilized distilled water served as control. The severity of the infections was assessed 60 days after transplantation. Using the scale described by Shanmugam *et al.,*[28] the Percentage Disease Index (PDI), which measures wilt incidence, was calculated.

0 = no symptoms;

1= ≤ 25% of the leaves with symptoms;

2 = 26–50% of the leaves with symptoms;

3 = 51–75% of the leaves with symptoms; and

4 = 76–100% of the leaves with symptoms[24].

Percent Disease Index (PDI) was calculated by the formula (equation 3) described by Wheeler[33].

$$PDI = \frac{\text{Sum of all disease rating}}{\text{Total no of fruits observed} \times \text{Maximum disease grade}} \times 100 \quad (3)$$

Percent disease control (PDC) over check calculated by formula (equation 4) described by Singh *et al.,*[29].

$$PDC = \frac{\text{Disease Severity in Check} - \text{Disease severity in Treatment}}{\text{PDI in check}} \times 100 \quad (4)$$

Statistical analysis :

The collected data were statistically assessed using the analysis of variance method (ANOVA), which was appropriate for CRD for laboratory and pot experiments and RCBD for field experiments, with the use of Web Agri Stat Package 2.0 (WASP). Microsoft Excel was used for data entry and normalization as well as figure production. The F-test in ANOVA was used to figure out whether there were significant differences between treatments, and the treatment averages were compared using the Least Significant Difference (LSD) at P≤0.05. Different letters were employed to illustrate substantial variations between treatments of findings obtained at the same time interval.

Morphological and molecular characterization of soil isolated Fungi :

Aspergillus niger (Sg9) and *Fusarium oxysporum* (Db4) isolated from the soil. The most important source of fungal isolation is soil. Thus, Chandrashekar *et al.,*[6] in isolated and identified ten species belonging to three genera (*Aspergillus, Penicillium, and Mucor*) from rhizosphere soils in different agricultural fields of Nanjangud taluk of Mysore district, Karnataka, India. Our findings shown in Fig. 1 exhibits the morphological character of isolated fungi[6]. Colony morphology of *A. niger* (Sg9), which exhibits a black colony is shown in Fig 1(a). Fig. 1(b) depicts the morphological character

of *F. oxysporum* (Db4) which exhibit pale purple colour surface. Similar morphological findings of both *A. niger* and *F. oxysporum* were observed by Alsohaili *et al.,*[5].

Table-1. exhibits the molecular characterization of two isolated fungus subjected to 18s rRNA sequence analysis. ITS sequence of Sg9 was submitted to the NCBI GenBank with the accession number OK338060. Phylogenetic identification (Fig. 2a) revealed sequence of Sg9 and *A. niger* isolate MK461010.1 are 87% similar. Similarly, the Db4 ITS sequence was deposited as accession no. OK338501. The similarities between the Db4 ITS nucleotide sequence and the *F. oxysporum* isolate MH259174 sequences acquired from the GenBank database had a 90% similarity (Fig. 2b).

Characterization of Biosynthesized ZnO NPs :

A) *UV-Visible Spectrophotometer (UV-Vis) and UV-Visible Diffuse Reflectance Spectra (DRS) Analysis:*

The fabrication of ZnO NPs was confirmed by UV-Visible spectroscopy. Figure 3 illustrates the absorption spectrum of synthesized ZnO NPs, which demonstrates the transformation of the zinc nitrate to the final product ZnO NPs. The existence of ZnO NPs synthesized by Sg9 fungi in culture filtrate is confirmed by an absorption peak at 312 nm (Fig. 3a) and ZnO NPs synthesized by Db4 at 315 nm (Fig 3b), which correlates to the intrinsic band-gap of Zn-O absorption. ZnO NPs have most prominent peaks at 300 and 359 nm[30]. The observed absorption peaks of the ZnO NPs are consistent with a recent investigation, which indicated an absorbance peak between 310 nm and 360 nm of wavelength[27]. According to Kalpana *et al.,*[19] the obtained absorption peak appeared to be similar to the absorption band[29]. Our findings are consistent with a study of Sasani *et al.,*[27] 2017 that analysed the UV spectrum range of ZnO NPs from 310–360 nm and is a distinguishing characteristic of pure ZnO NPs[27].

UV-Visible DRS was used to measure the optical band gap of ZnO NPs shown in Fig. 4. The highest reflectance occurring at a wavelength of 346 nm with energy gap 3.5 eV for Sg9-ZnO NPs (Fig. 4a and b). Similarly, the DRS absorption of Db4-ZnO NPs was found to be 339 nm along with the band gap of 3.8 eV (Fig. 4c and d). The findings of Hajiashrafi and Kazemi 2019 declare that the DRS absorption spectra of ZnO NPs exhibited an absorption peak in the 200-400 nm range[10]. Further, the Kubelka-Munk (K-M theory) hypothesis was used to identify the absorption band of the NPs produced (equation 5).

$$F(R\infty) = 1 - R\infty / 2R\infty \quad (5)$$

Where, $(F(R)E)^{1/2}$ intercept plots against photon energy deliver bandgap and $R\infty$ is the reflection coefficient.

B) *FTIR analysis :*

The details of the chemical interaction between Zn and O provided by the FTIR spectrum study is deposited in Fig. 5. FTIR spectra of synthesized ZnO NPs using Sg9 are shown in Figure 5a. The hydroxyl group O-H stretching is responsible for the big peaks at 3452.44 cm^{-1}. Asymmetrical stretching of the zinc carboxylate causes wide banding peaks at 1631.05 cm^{-1}. A peak in the symmetric

Table-1. Molecular characterization of *Aspergillums niger* (Sg9) and *Fusarium oxysporum* (Db4) with 18s rRNA sequences deposited to GenBank, NCBI

Sl. No.	Code of organisms	Code	Name of organisms	Accession no.
1	KUMBASBT-63	Sg9	*Aspergillus niger*	OK338060
2	KUMBASBT-58	Db4	*Fusarium oxysporum*	OK338501

Table-2. *In vitro* Screening of Sg9 and Db4 ZnO NPs Against *Colletotrichum fructicola*

Concentration	25 ppm	50 ppm	100 ppm	250 ppm	500 ppm	750 ppm	1000 ppm	2000ppm
Treatments	Mycelial diameter (cm)							
Sg9-ZnoNPs	6.6	5.0	4.1	3.0	2.0	1.3	0.8	0.5
Db4-ZnoNPs	6.5	5.4	4.5	3.2	2.4	1.5	1.1	0.5
Std (Propiconazole): 1000 ppm: 2.1mm							Control : 7.7mm	

Table-3. Mycelial Growth Inhibition (%) of Sg9 and Db4 ZnO NPs Against *C. fructicola*

Concentration	25 ppm	50 ppm	100 ppm	250 ppm	500 ppm	750 ppm	1000 ppm	2000 ppm	Std (Propi-conazole) 1000 ppm
Treatments	Mycelial growth inhibition (%) after15 DAT								
Sg9-ZnoNPs	14.29	35.06	47.19	60.61	74.03	83.55	89.61	93.51	73.16
Db4-ZnoNPs	15.58	29.44	41.13	58.87	68.40	80.95	85.71	93.51	73.16

Table-4. Effect of Sg9 and Db4 ZnO NPs on Lesion size caused by *Colletotrichum fructicola*

Treatment	Lesion size in mm					
	Nanoparticles applied before inoculation			Nanoparticles applied after inoculation		
Concentration	500 ppm	750 ppm	1000 ppm	500 ppm	750 ppm	1000 ppm
Sg9-ZnoNPs	15.46^{d}	11.23^{c}	0.36^{a}	19.45^{c}	18.53^{b}	3.01^{a}
Db4-ZnoNPs	22.45^{g}	19.45^{f}	18.02^{e}	23.02^{e}	22.02^{d}	19.88^{c}
Std :Propiconazole	4.85^{b}			7.56^{a}		
Control	23.4^{h}	23.4^{h}	23.4^{h}	23.4^{f}	23.4^{f}	23.4^{f}
SEm +/-	0.060			0.065		
CD at 5 %	0.428			0.447		
CV	1.696			1.491		

Table-5. Percentage disease control of Sg9 and Db4 ZnO NPs *Colletotrichum fructicola*

Treatment	Percent disease control (%)					
	Nanoparticles applied before inoculation			Nanoparticles applied after inoculation		
Concentration	500 ppm	750 ppm	1000 ppm	500 ppm	750 ppm	1000 ppm
Sg9-ZnoNPs	33.93	52.01	98.46	16.88	20.81	87.14
Db4-ZnoNPs	4.06	16.88	22.99	1.62	5.9	15.04
Std: Propiconazole			79.27			67.69

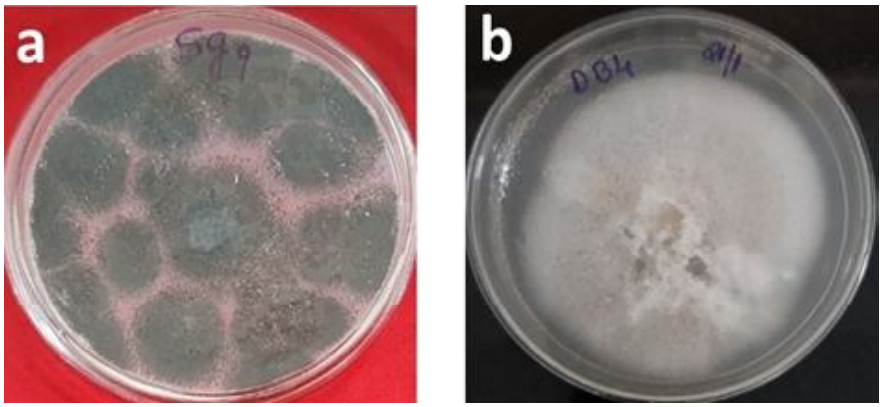

Fig. 1. Morphological identification of isolated (a) *Aspergillus niger* (Sg9) and (b) *Fusarium oxysporum* (Db4)

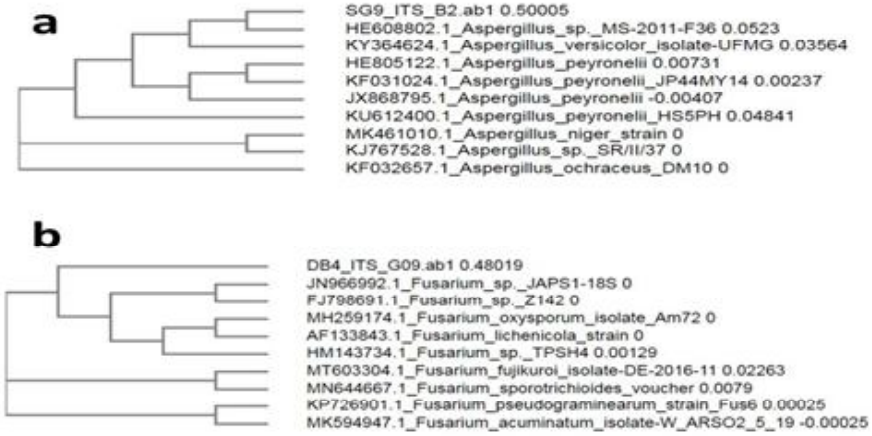

Fig. 2. Phylogenetic tree of (a) *Aspergillums niger* (Sg9) & (b) *Fusarium oxysporum* (Db4)

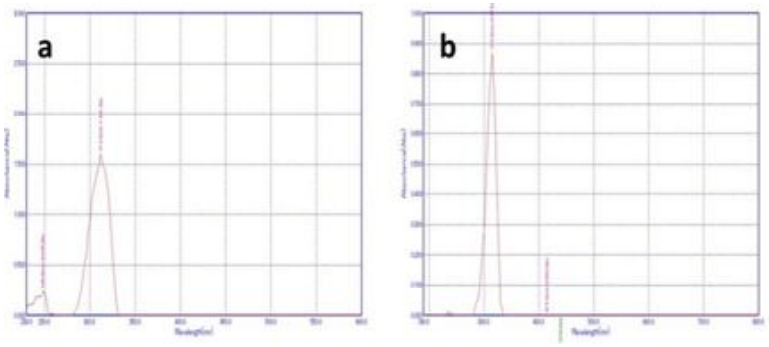

Fig. 3. UV-Visible Spectroscope a) Sg9-ZnO NPs and b) Db4-ZnO NPs

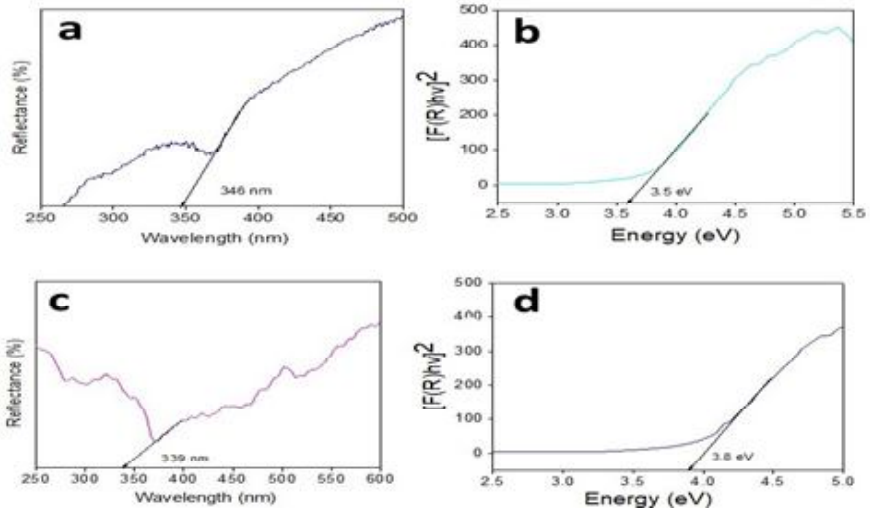

Fig. 4. UV-Visible DRS of a) Sg9-ZnO NPs and c) Db4-ZnO NPs, Band gap energy of b) Sg9-ZnO NPs and d) Db4-ZnO NPs

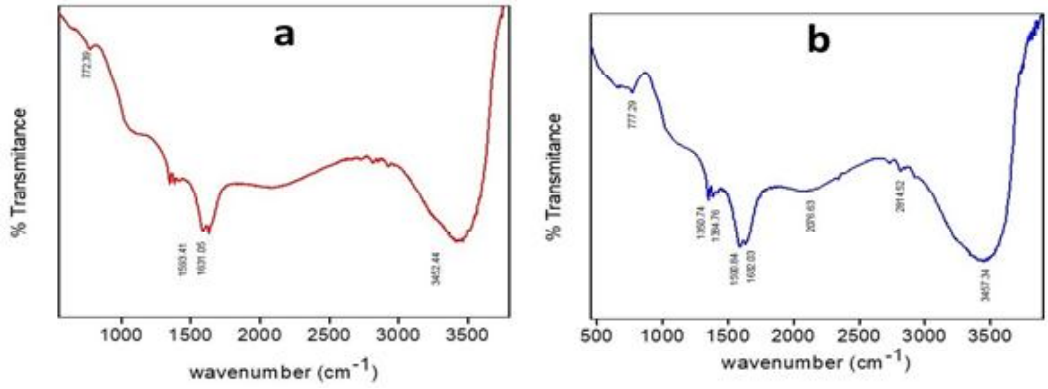

Fig. 5. FTIR Spectra of a) Sg9-ZnO NPs and (b) Db4-ZnO NPs

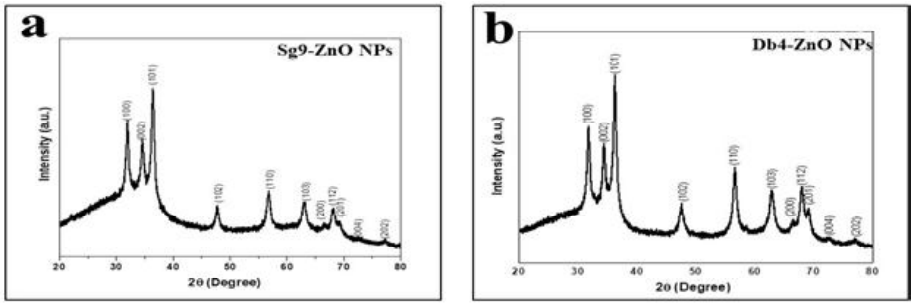

Fig. 6. XRD Spectra of a) Sg9-ZnO NPs and b) Db4-ZnO NPs

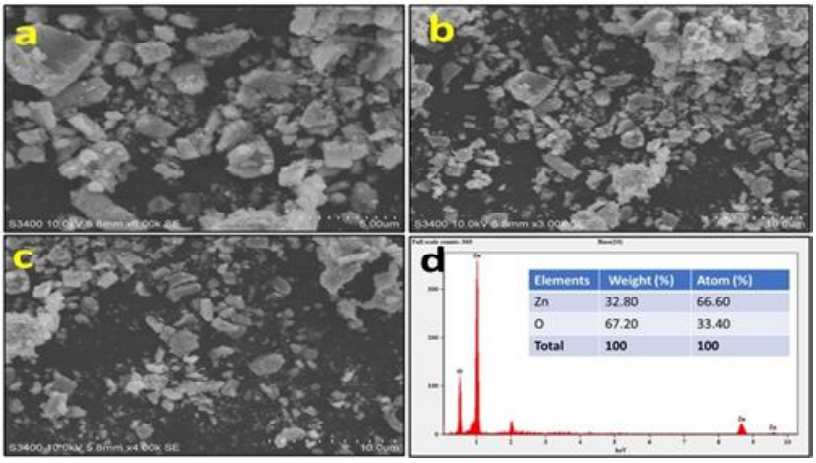

Fig. 7. (a-c) SEM images of Sg9-ZnO NPs, (d) EDS analysis of Sg9-ZnO NPs

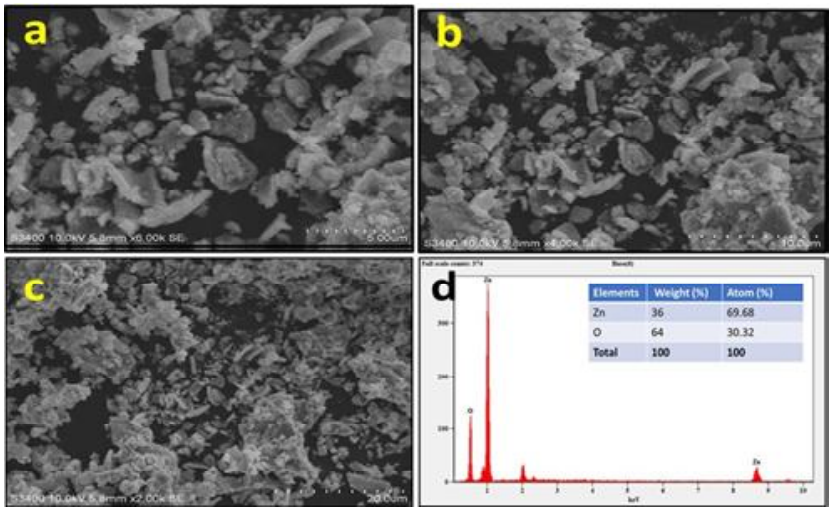

Fig. 8. (a-c) SEM images of Db4-ZnO NPs, (d) EDS analysis of Db4-ZnO NPs

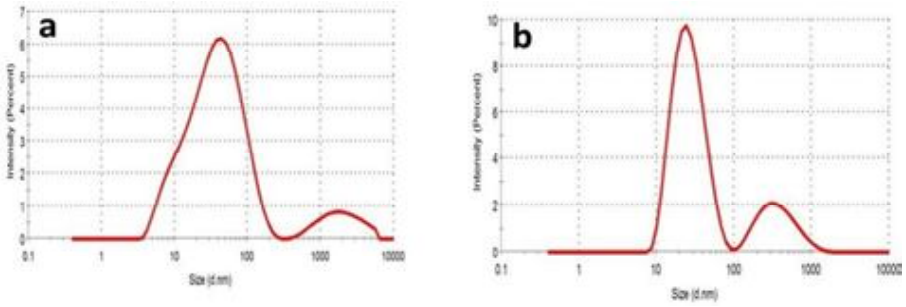

Fig. 9. Dynamic Laser Scattering of (a) Sg9- ZnO NPs and (b) Db4-ZnO NPs

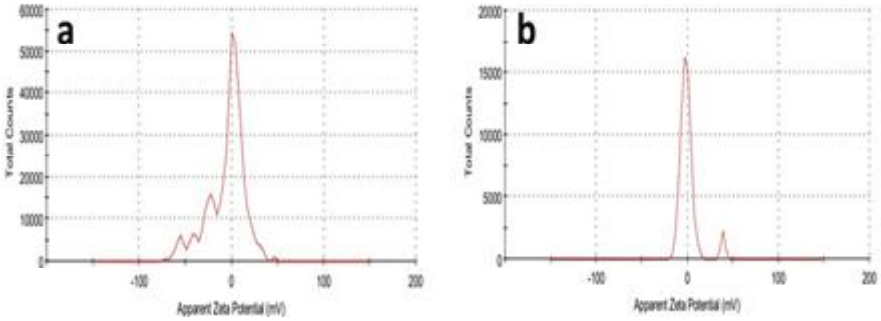

Fig. 10. Zeta potential of (a) Sg9- ZnO NPs and (b) Db4-ZnO NPs

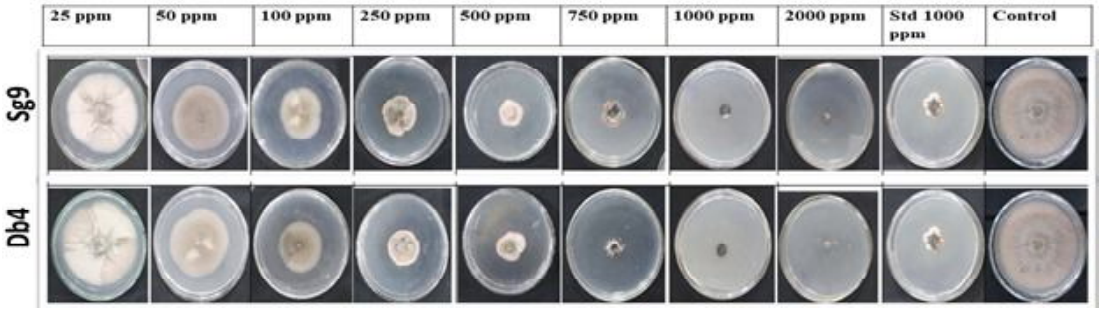

Fig. 11. *In vitro* Screening of Sg9 and Db4 ZnO NPs Against *Colletotrichum fructicola*

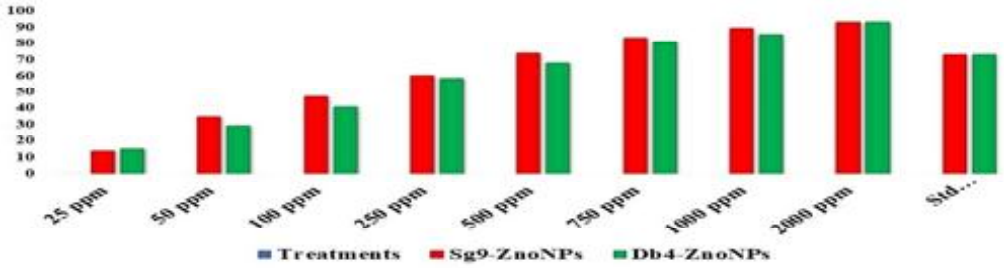

Fig. 12. Mycelial Growth Inhibition (%) of Sg9 and Db4 ZnO NPs Against *C. fructicola*

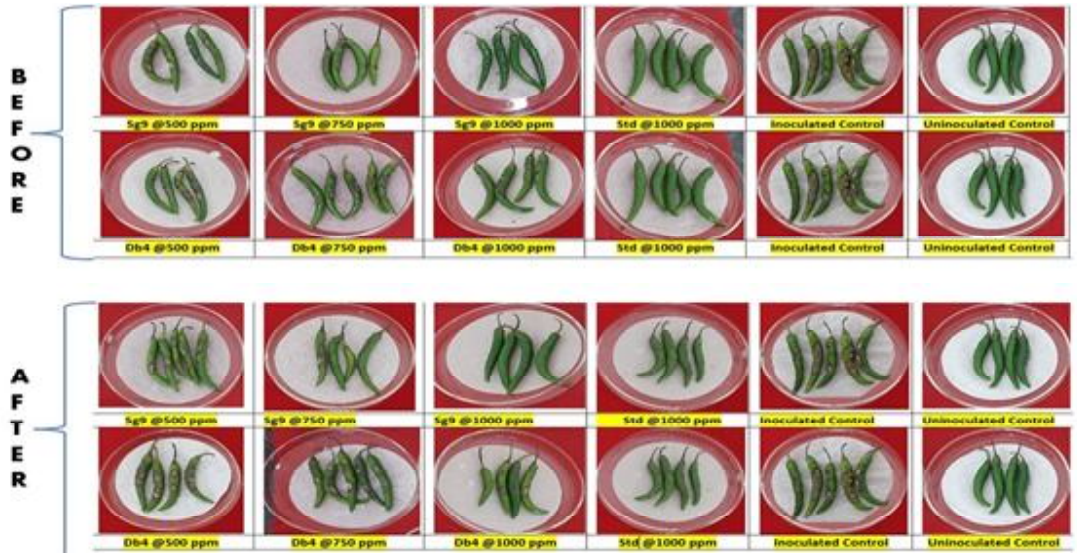

Fig. 13. Effect of Sg9 and Db4 ZnO NPs on Lesion size caused by *C. fructicola*

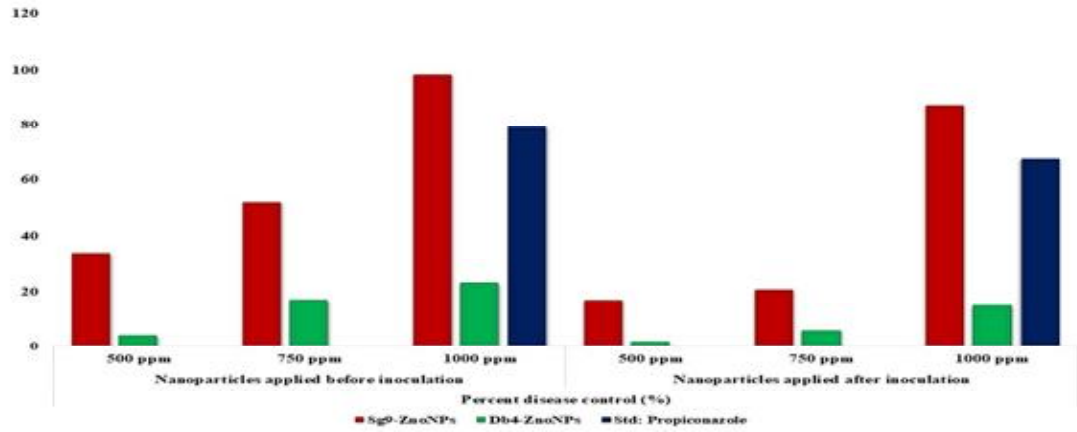

Fig. 14. Percentage disease control of Sg9 and Db4 ZnO NPs *Colletotrichum fructicola*

bending vibration of ZnO around 772.39 cm^{-1}. 1593 cm^{-1} is assigned to asymmetric carboxyl groups due to the weak vibration of ZnO.

Fig. 5b depicts the FTIR spectrum of Db4-ZnO NPs. The hydroxyl (O-H) group of water stretching and banding modes is typically responsible for broad bands at 3457.34 and 1632.03 cm^{-1}. Metal-oxygen vibrations of ZnO are still identified at 777.29 cm^{-1}. The CH stretching vibration causes the peaks at 2814.52 and 2076.63 cm^{-1}. Asymmetric carboxyl groups are responsible for the signal at 1590.84 cm^{-1}. C-C stretching causes the

peaks at 1384.76 and 1350.74 cm^{-1}.

All the obtained peaks were in accordance with Jeyaleela *et al.,* 2020 in which peak O-H bending vibration of 3334.71 cm^{-1} and at 1656.36 cm^{-1} axial stretching band O is visible[18].

C) *XRD Anlaysis :*

XRD pattern of *A. niger* Sg9-ZnO NPs is deposited in Fig. 6 a. The assignment of the ZnO NPs diffraction peaks to (100), (002), (101), (102), (110), (103), (200), (201), (004), and (202) was verified for 2θ= 32.21°, 34.73°, 36.44°, 47.71°, 56.85°, 63.21°, 66.26°, 68.38°, 69.36°, and 72.76°. All of the ZnO NPs diffraction peaks have a hexagonal phase and wurtzite behavior, match perfectly with JCPDS file No. 3-888. As a result, Sg9-ZnO nanoparticles turned out to have a fine crystalline structure as evidenced by the sharper and stronger diffraction peaks, with an average crystal size of 30 nm.

Similarly, Figure 6b depicts the XRD pattern of Db4-ZnO NPs. It was confirmed that each of the ZnO NPs diffraction peaks at 2θ = 31.77°, 34.46°, 36.31°, 47.54°, 56.72°, 62.95°, 68.12°, 69.17°, 72.76°, and 77.00° can be associated with (100), (002), (101), (102), (110), (103), (200), (201), and (004). All of the ZnO NPs' diffraction peaks exhibit a hexagonal phase in a wurtzite-like fashion when compared to JCPDS file No. 76-704. Sharp diffraction peaks indicate that ZnO NPs were crystalline, and it was later discovered that the average crystal size was 29 nm. Likewise, the XRD patterns of both Sg9 and Db4 ZnO NPs additionally demonstrate no impurity peaks, indicating purity and good crystallinity. The XRD results are compatible with previous studies which revealed multiple peaks at 2 between 31.77° and 98.67° and include consistent results from XRD examination of ZnO NPs synthesized using biological sources[17,22].

D) *SEM-EDS analysis :*

To investigate the morphology of the Sg9-ZnO NPs and Db4-ZnO NPs SEM images with different magnifications are shown in Figure 7 (a-c) and 8 (a-c). The SEM images of both Sg9-ZnO NPs and Db4-ZnO NPs clearly show the irregular surface morphology with different sized particles due to agglomeration this in return indicates the larger surface area which was reported by Al-Kordy *et al.,*[4].

Further, the EDS analysis of Sg9-ZnO NPs and Db4-ZnO NPs are exhibited in Figure 7d and 8 d which confirms the purity of the synthesized ZnO NPs and no other impurity. For Sg9-ZnO NPs, the exact Zn and O atomic percentage elements were found to be 66.60% and 33.40% along with the percentage elemental composition was observed to 32.80% and 67.20%. Likewise, Db4-ZnO NPs show the 69.68% and 30.32% of the atomic percentage of elements meanwhile, the percentage of elements Zn and O was observed to be 36% and 64 %. These findings were in accordance with the previous existing report of Hasnidawani *et al.,*[11].

E) *Dynamic laser scattering and Zeta potential analysis :*

Dynamic Laser Scattering (DLS) represents the particle size carried out using

the dynamic light scattering technique at 173º scattering angle at room temperature From the DLS analysis, the synthesized Sg9 and Db4 ZnO NPs are in the nanometer range having smaller size particles with the average size of 29.29 nm and 26.33 nm (Figure 9a and b). The size parameters are well estimated and there are generally larger particles, according to the DLS observations. The synthesized NPs were well matching with the previous report of Abdelaziz *et al.,* 2022 which declares that the average size ranges between 3.50 and 67.30 nm [3]. The findings of Mekky *et al.,*[21] declare that ZnO NPs prepared from *A. niger* extracellular extracts have a size distribution of 84.79 nm[21].

Further, the Zeta potential of Sg9 and Db4 ZnO NPs are depicted in Figure 10a and b. Zeta potential of the NPs reveals the stability and surface charge on the surface of particles. The observed potential of Sg9 and Db4 ZnO NPs was -5.17 mV and 0.471mV. In general, the greater the absolute value of zeta potential (either +ve or -ve), the greater the repulsion between the particles to be aggregated. As a result, the greater the stability of the NPs *i.e.*, particles with zeta potentials greater than ±30mV are typically considered stable[8]. As the Sg9 and Db4 ZnO NPs were found to be between ±30mV, the ZnO NPs are considered as highly stable.

In vitro Screening of ZnO NPs Against C. fructicola :

The effect of Sg9 and Db4 ZnO NPs on *C. fructicola* mycelial growth is depicted in Table 2. Evaluation of the data revealed that increasing the NP content considerably lowers *C. fructicola* mycelial growth. The mycelial growth for 2000 ppm and 1000 ppm was observed to be 0.5 and 0.8 mm for Sg9-ZnO NPs, whereas for Db4-ZnoNPs the growth was observed to be 0.5 and 1.1 mm for 2000 ppm and 1000 ppm. The inhibition checks for standard Propiconazole (1000 ppm) and the control was observed to be 2.1 mm and 7.7 mm which statistically showed less inhibition compared to the 1000 ppm ZnO NPs ie., 0.8 and 1.1 mm (Fig. 11). Further, the data reveals that from 25 to 250 ppm had no effective inhibition in the mycelial growth. The percentage inhibition of mycelial growth is shown in Figure 12 where the highest inhibition was observed to be 93.51% and 89.61% for Sg9-ZnO NPs, whereas for Db4-ZnoNPs the highest inhibition was observed to be 93.51% and 85.71% for 2000 and 1000 ppm (Table-3). The obtained results suggest that biologically synthesized Sg9 and Db4 ZnO NPs are statistically superior in the inhibition of *C. fructicola* mycelial growth. Iliger *et al.,*[15] declare that as nanoparticle concentration elevated from 25 to 1000 ppm, test fungal mycelial growth greatly reduced[15].

In vivo screening of ZnO NPs against Colletotrichum fructicola on Chilli fruits :

In vivo, screening of ZnO NPs against *C. fructicola* was performed at three different concentrations 500, 750 and 1000 ppm along with a standard check using Propiconazole. This was performed by treating the NPs before the inoculation of the pathogen and after the inoculation of pathogens to the chilly fruits (Table-4). The findings demonstrated that treatment of NPs before pathogen

inoculation can achieve much greater suppression of *C. fructicola* than spraying NPs following pathogen inoculation. Results clearly show that *C. fructicola* lesion size on chili fruit can be greatly reduced by NPs as compared with conventional fungicides (Figure 13). The data in Table 4 show that Sg9 and Db4 ZnO NPs at 500, 750, and 1000 ppm applied before-inoculation and after-inoculation completely inhibited the disease and there were no lesions on fruits treated with Sg9-ZnO NPs, whereas Db4-ZnO NPs treated chilly fruits showed less inhibition of the lesions in comparison to Sg9-ZnO NPs. Figure 14 shows the percentage of disease control of ZnO NPs before and after inoculation of pathogens. The Sg9-ZnO NPs for 1000-ppm treatment showed 98.46% and 87.14% for pre and post-inoculation of the pathogen. Similarly, Db4-ZnO NPs for 1000 ppm showed 22.99% and 15.04% (Table-5). The results declare that the Sg9-ZnO NPs are more effective than standard checks in controlling the disease in both pre and post pathogen inoculation, whereas Db4-ZnO NPs had less inhibition effect on the pathogen for pre and post inoculation. The results well match with the previous reports of Iliger *et al.,*[15] which declared that in the detached fruit approach, NPs applied before pathogen inoculation produced better results than pathogen after-inoculation in terms of incubation length, lesion number, and lesion size[15,23].

In our study, the isolation of Sg9 and Db4 fungi was successful and subjected to molecular characterization sequencing. Later the novel synthesis of Sg9 and Db4 ZnO NPs was performed using the isolated fungicides. The synthesized ZnO NPs were characterized and subjected to *in vitro* and *in vivo* analysis for the control of the pathogen *C. fructicola* that causes fruit rot and are considered destructive diseases leading to decreased growth and death of most infected chilly fruits. The observations depicted that the pathogens treated with the synthesized nanoparticles had shown the prevention of diseases for the chilly fruits. To summarize, NPs particularly ZnO NPs show immense potential for reducing the prevalence of fungal diseases and boosting plant growth, as well as offering a new scientific basis for fungal disease prevention and control. As a result, it may be claimed that tested treatments are successful in combating the disease, affordable, and secure. Thus, these NPs could be utilized commercially to manage Chilli fruit rot disease caused by *Colletotrichum fructicola*.

Controlling chilli fruit rot diseases using biologically synthesized ZnO NPs could include further optimization of nanoparticle synthesis methods, extensive field trials to evaluate long-term effects, assessment of potential environmental impacts, and exploration of different application techniques for improved efficacy and cost-effectiveness.

References :

1. Abdelaziz, A.M., S.S.Salem, A.M.A. Khalil, D.A. El-Wakil, H.M Fouda and A.H Hashem (2022). *Biometals. 35*(3): 601-616.
2. Ahmad, M., A. Ali, Z. Ullah, H. Sher., D.Q. Dai, M. Ali, J. Iqbal, M. Zahoor and I. Ali (2022). *Front Bioeng Biotechnol. 10:*

988607.

3. Aldalbahi, A., S. Alterary, R. Ali Abdullrahman Almoghim, M.A. Awad, N.S. Aldosari, S. Fahad Alghannam, A. Nasser Alabdan, S. Alharbi, B. Ali Mohammed Alateeq, A. Abdulrahman Al Mohsen, M.A. Alkathiri and R. Abdulrahman Alrashed (2020). *Molecules; 25*(18): 4198.
4. Al-Kordy, H.M.H., S.A. Sabry and M.E.M. Mabrouk (2021). *Sci Rep; 11*(1): 10924.
5. Alsohaili, S. (2018). *Journal of Essential Oil Bearing Plants; 21*(1): 139–45.
6. Chandrashekar, M.A., K.S. Pai and N.S. Raju (2014). *Int. j. curr. microbiol. appl. sci.; 3*(5): 559-66.
7. Choudhury. S. R., M. Ghosh, A. Mandal, D. Chakravorty, M. Pal, S Pradhan and A. Goswami (2011). *Appl Microbiol Biotechnol; 90*(2): 733-43.
8. Ganeshkar, M.P., P.H. Goder, M.R. Mirjankar, A.T. Gaddigal, P. Shivappa, C.M. Kamanavalli (2022). *Inorganic and Nano-Metal Chemistry;* 1–14.
9. Hagfeldt, A and Grätzel M (2000). *Acc Chem Res.; 33*(5): 269-77.
10. Hajiashrafi S. and N. Motakef Kazemi (2019). *Heliyon.* 2019; *5*(9): e02152. doi: 10.1016/j.heliyon.e02152.
11. Hasnidawani J.N., H.N. Azlina, H. Norita, N.N. Bonnia, S. Ratim and E.S. Ali (2016). *Procedia Chemistry; 19:* 211–6.
12. Hidayat, C., E.Sumiati, Wina, A. Jayanegara (2021). IOP Conference Series: *Earth and Environmental Science; 888*(1): 012056.
13. Hingorani, S., V. Pillai, P.Kumar, M.S. Multani and D.O. Shah (1993). *Materials Research Bulletin; 28*(12): 1303–10.
14. Hsueh, Y.H., W.J. Ke, C. T. Hsieh, K.S. Lin KS, D.Y. Tzou and C.L. Chiang (2015). *PLoS One.; 10*(6): e0128457.
15. Iliger K.S., T.A. Sofi, N.A. Bhat, F.A. Ahanger, J.C. Sekhar, A.Z. Elhendi, A.A. Al-Huqail and F. Khan (2021). *Saudi J Biol Sci.; 28*(2): 1477-1486.
16. Jackson .J.B., S.L. Westcott, L.R. Hirsch, J.L. West and N.J. Halas (2003). *Applied Physics Letters; 82*(2): 257–9.
17. Jain. D. Shivani., A.A. Bhojiya, H. Singh, H.K. Daima, M. Singh, S.R. Mohanty, B.J. Stephen and A. Singh (2020). *Front Chem.* Sep 30; *8:* 778.
18. Jeyaleela. G.D., J.R. Vimala, S.M. Sheela, A. Agila, M.S. Bharathy and M. Divya (2020). *Oriental Journal of Chemistry; 36*(04): 655–64.
19. Kalpana. V.N., B.A. Kataru, N. Sravani, T. Vigneshwari, A. Panneerselvam and V. Devi Rajeswari (2018). *Open Nano; 3:* 48–55.
20. Mahlambi. M.M., A.K. Mishra, S.B. Mishra, A.M. Raichur, B.B. Mamba and R.W. Krause (2012). *Journal of Nano-materials;* 1–12.
21. Mekky. A.E., A.A. Farrag, A. A. Hmed, A.R Sofy (2021). *Journal of Pure and Applied Microbiology; 15*(3): 1547–66.
22. Nazir. S., M. Zaka, M. Adil , B.H. Abbasi and C. Hano (2018). *IET Nanobio-technol; 12*(5): 604-608.
23. Parey. M.A., V.K. Razdan, T.A. Sofi (2013). *Int. j. agric. crop sci; 5*(7): 723.
24. Raliya .R, I. Rathore, J.C. Tarafdar (2013). *Journal of Bionanoscience; 7*(5): 590–6.
25. Raliya. R and J.C. Tarafdar (2014).

International Nano Letters.; 4(1).

26. Raut R.W., V. D. Mendhulkar, and S. B. Kashid (2014). *J. Photochem Photobiol B.; 132:* 45-55.
27. Sasani Ghamsari. M., S. Alamdari, W. Han and H.H. Park (2016). *Int J Nanomedicine. 12:* 207-216.
28. Shanmugam. V., K. Atri, S. Gupta, N. Kanoujia and D.S. Naruka (2011). *Folia Microbiol (Praha); 56*(2): 170-7.
29. Singh RB, HK Singh and A. Parmar (2014). *Pakistan J of Biol Sci*; *17*(4): 511-51.
30. Thakkar. K.N., S.S. Mhatre and R.Y. Parikh (2009). Biological synthesis of metallic nanoparticles. *Nanomedicine. 2010* Apr; *6*(2): 257-62. doi: 10.1016/j.nano.2009.07.002.
31. Topoglidis. E, A.E.G. Cass, O'Regan and J.R. Durrant JR. (2001). *Journal of Electroanalytical Chemistry; 517*(1–2): 20–7.
32. Vinila. V.S and J. Isac (2022). Synthesis and structural studies of superconducting perovskite gdba2ca3cu4o10.5+δ nanosystems. *Design, Fabrication, and Characterization of Multifunctional Nanomaterials;* 319–41.
33. Wheeler BE. (1969). An introduction to plant diseases. An introduction to plant diseases.
34. Wu. H., R. Yang, B. Song, Q. Han, Li J, Y. Zhang, Y. Fang, R. Tenne and C. Wang (2011) Biocompatible inorganic fullerene-like molybdenum disulfide nanoparticles produced by pulsed laser ablation in water. *ACS Nano. 22*;5(2): 1276-81. doi: 10.1021/nn102941b. Epub 2011 Jan 11.